Scripta Materialia 218 (2022) 114810

Contents lists available at ScienceDirect

Scripta Materialia

journal homepage: www.journals.elsevier.com/scripta-materialia

Interaction between a dislocation and nanotwin–hcp lamella in Ni-based concentrated alloys from atomistic simulations

Sho Hayakawa, Haixuan Xu *

Department of Materials Science and Engineering, The University of Tennessee, Knoxville, TN 37996, United States

ARTICLE INFO

Keywords:
High-entropy alloy
Molecular dynamics
Dislocation
Ductility
Plastic deformation

ABSTRACT

We investigate the fundamental interaction between a dislocation and nanotwin–hexagonal close-packed (hcp) lamella in Ni-based concentrated alloys using molecular dynamics simulations. We identify two types of interaction modes that have different contributions to the ductility: the lamella either transmits or absorbs the dislocation. Furthermore, the dominant interaction mode changes with an increase in the interaction's critical stress, which exhibits a strong dependence on a material parameter related to the stacking fault energy. The combination of the dominant mode and critical stress dependences could lead to the simultaneous increase in the strength and ductility with decreasing temperature in NiCoCr. Additionally, it is found the type of interaction mode to occur is influenced by the hcp lamella thickness, which could further enhance the ductility, together with the unique mechanism of the dislocation absorption. The obtained insights would be useful for the fundamental understanding of the intriguing properties of Ni-based concentrated alloys.

In recent years, medium- and high-entropy alloys (M/HEAs) have attracted a substantial amount of attention as an interesting class of materials [1–3]. One of the characteristic features of these alloys is that they contain approximately equal atomic concentrations of the constituent elements. Furthermore, some of the alloys crystalize as single-phase solid solutions with a simple crystal structure, rather than producing intermetallic phases [4–9]. Many studies have focused on these single-phase alloys and reported intriguing properties of some systems that are desirable for structural applications. For instance, it has been confirmed that NiCoCrFeMn quinary HEAs exhibit high strength and ductility, and they further improve simultaneously as the temperature decreases [5–7], which is a rare phenomenon in conventional dilute alloys. Experimental studies have reported deformation twinning was observed at cryogenic temperatures in these alloys [5,7,9], which could trigger their enhanced ductility because it would work as an additional deformation mode. A recent computational study [10] found a temperature-dependent mechanism of the interaction between a dislocation and coherent twin boundary (CTB) that could also contribute to the unusual temperature dependence of their ductility. In addition, subset alloys of NiCoCrFeMn HEAs have been extensively investigated [9–13]. It has been revealed that NiCoCr MEAs also crystalize as single-phase solid solutions, and importantly, they possess better cryogenic strength, ductility, and fracture toughness than other subsets and even the parent alloy NiCoCrFeMn HEAs [11,14]. Although this is a very interesting observation and could be critical to clarify the underlying mechanism of the intriguing behavior of M/HEAs, the exact origin has remained unclear.

Extensive investigations of deformation mechanisms in NiCoCr MEAs have been carried out [15–22], and some of them reported key observations of microstructural features. For instance, the formation of lamella structures with hexagonal close-packed (hcp) phase were observed along twin boundaries during deformation process [17–20]. Furthermore, Niu et al. [17] directly compared microstructures of NiCoCr MEAs and NiCoCrFeMn HEAs under deformation and confirmed the nanotwin–hcp lamella structure only exists in NiCoCr. It is noted that the lamella structures were also observed in NiCoCrFeMn previously but it was under high pressure conditions [23,24]. Density functional theory (DFT) calculations [17] suggested unique magnetic configurations of NiCoCr MEAs could lead to the exclusive formation of the hcp lamellas in these alloys while the formation would be suppressed by magnetic frustration due to Mn in NiCoCrFeMn HEAs and other ternary derivatives. Since the hcp lamellas would work as strong barriers for dislocation motion, these structures could be relevant to the strength and ductility of NiCoCr. Indeed, Slone et al. [20] constructed mean-field and full-field models for hardening behavior of NiCoCr and found nanotwin–hcp lamellas could contribute to significant hardening, which

* Corresponding author: 336 Ferris Hall, 1508 Middle Drive, Knoxville, TN 37996, United States.
E-mail address: xhx@utk.edu (H. Xu).

https://doi.org/10.1016/j.scriptamat.2022.114810
Received 2 February 2022; Received in revised form 14 April 2022; Accepted 12 May 2022
Available online 20 May 2022

might be associated with dislocation–hcp lamella interactions. Therefore, it is essential to investigate the underlying mechanism of these interactions. A previous study [17] performed atomistic simulations to investigate the interaction between a dislocation and hcp lamella in face-centered cubic (fcc) systems. However, they focused on static conditions alone while employing an interatomic potential for fcc Co as a surrogate system for NiCoCr, and extensive investigations have not been reported yet. More importantly, possible effects of the interaction on the strength and ductility of the system at finite temperatures have remained unclear.

In this study, we perform molecular dynamics (MD) simulations of the interaction between a dislocation and a nanotwin–hcp lamella in Ni-based concentrated alloys. Particularly, we study NiCo, NiFe, NiCoCr, and NiCoCrFe alloys as well as pure Ni for comparison. In addition, we focus on a screw dislocation as a fundamental case of the dislocation–hcp lamella interaction. We investigate the interaction mechanism, its critical stress, and the influences of the thickness of the hcp lamella on the interaction in detail. Furthermore, we discuss possible contributions of the interaction to the unusual temperature dependence of the superior strength and ductility of NiCoCr .

Fig. 1(a) shows the simulation setup employed in this study. The original grain is oriented along the [112], $[\bar{1}\bar{1}1]$, and $[1\bar{1}0]$ directions, and a twin grain is created beside it so that the two grains are separated by a $\Sigma3(111)[1\bar{1}0]$ CTB. In addition, we introduce an hcp lamella along the CTB in the twin grain by changing the pattern of the (111) layers stacking sequence. The cell lengths along the Y and Z directions are ~33 and ~4 nm, respectively, while that along the X direction is varied from ~34 to ~44 nm, depending on the hcp lamella thickness, which is set to 7, 31, and 55 atomic layers. Free boundary conditions are applied along the X and Y directions while a periodic boundary condition is applied along the Z direction. A screw dislocation with the Burgers vector parallel to the Z direction is introduced beside the CTB, following a manner described in [25]. When the system energy is minimized, the introduced dislocation dissociates into two Shockley partial dislocations with the Burgers vector of $a_0/6[2\bar{1}1]$ and $a_0/6[1\bar{2}1]$, respectively, where a_0 denotes the lattice constant. Two different interatomic potentials are employed for describing the interatomic interactions in the system because a previous study for the interaction between a screw dislocation and CTB reported the employed potential could influence the interaction behavior [26]. We use an embedding atom method-type potential for a binary alloy of NiFe developed by Bonny et al. [27] and an interatomic potential for NiCoCrFeCu by Farkas et al. [28]. We vary atomic compositions for the binary NiFe systems using the Bonny potential; while equiatomic alloys are employed for NiCo, NiCoCr, and NiCoCrFe using the Farkas potential. The constituent elements are randomly distributed for all the alloy systems, as shown in Fig. 1(b).

We employ a stress-controlled condition to induce the interaction between the dislocation and hcp lamella, the detail of which is described in the following: first, a shear stress is applied at the top and bottom XZ surfaces of the cell by superimposing atomic forces for several layers from the surfaces, which is followed by a system energy minimization. Note, the stress value here is carefully chosen so that it becomes sufficiently smaller than the critical stress for the interaction to occur. Then, the system temperature is raised to 77 K while keeping the stress. The temperature of 77 K is chosen because many experimental studies [5–7, 11,14] reported an excellent balance between the strength and ductility in Ni-based concentrated alloys at this particular temperature. It should be noted that the temperature increase here needs to be performed carefully to prevent the occurrence of the interaction before the system reaches an equilibrium state (the detailed procedure is presented in Supplementary material). Once the equilibrium state is obtained, we increase the stress at a constant rate of 0.25 MPa/ps until an interaction process occurs and completes. The microcanonical ensemble is employed after the equilibration, where we confirm the increase in temperature during the simulations is negligibly small. The time is integrated using the Verlet algorithm at a constant timestep of 2.0 fs. At each condition, over 15 repeated calculations are performed while changing the distributions of the constituent elements and initial atomic velocities to examine the statistical variation of the results. All the simulations in this study are carried out using the large atomic/molecular massively parallel simulator (LAMMPS) [29]. To investigate the interaction process, we employ the common neighbor analysis (CNA) [30] and visualize the obtained results using OVITO [31].

We observe two types of interaction modes in the simulations, as shown in Fig. 2, i.e., the lamella either transmits or absorbs the dislocation, which we call Mode I and Mode II in this study, respectively. The detailed process of each mode is described next. In Mode I, the dissociated dislocation firstly constricts and becomes a perfect dislocation (Fig. 2 (a-2)). Then, it starts to penetrate into the lamella while maintaining a perfect dislocation configuration (Fig. 2 (a-3)). When the dislocation reaches the other side of the lamella, it re-dissociates into two Shockley partial dislocations in the twin grain (Fig. 2 (a-4)), followed by the completion of the transmission process (Fig. 2 (a-5)). On the other hand, in Mode II, the dissociated dislocation also becomes a perfect dislocation firstly and starts to penetrate into the lamella, as in Mode I (Fig. 2 (b-2) and (b-3)). However, the perfect dislocation re-dissociates into Shockley partial dislocations at a certain point during the penetration (Fig. 2 (b-4)), and they immediately glide away from each other within the lamella (Fig. 2 (b-5)), resulting in a dislocation absorption process. Note that the point of the re-dissociation varies in

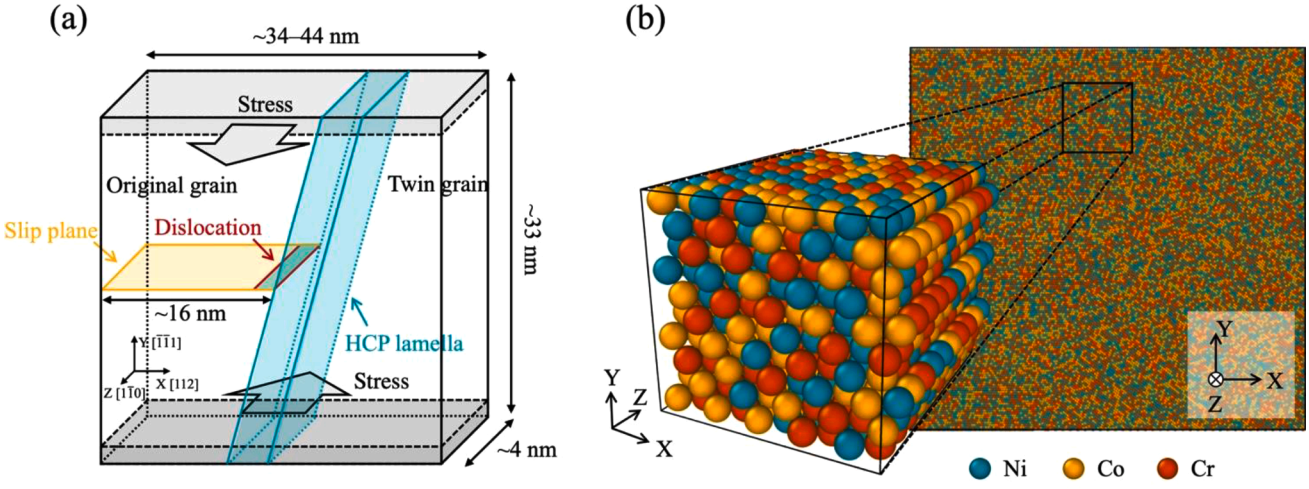

Fig. 1. (a) Simulation setup. (b) Representative atomic configuration of the NiCoCr system.

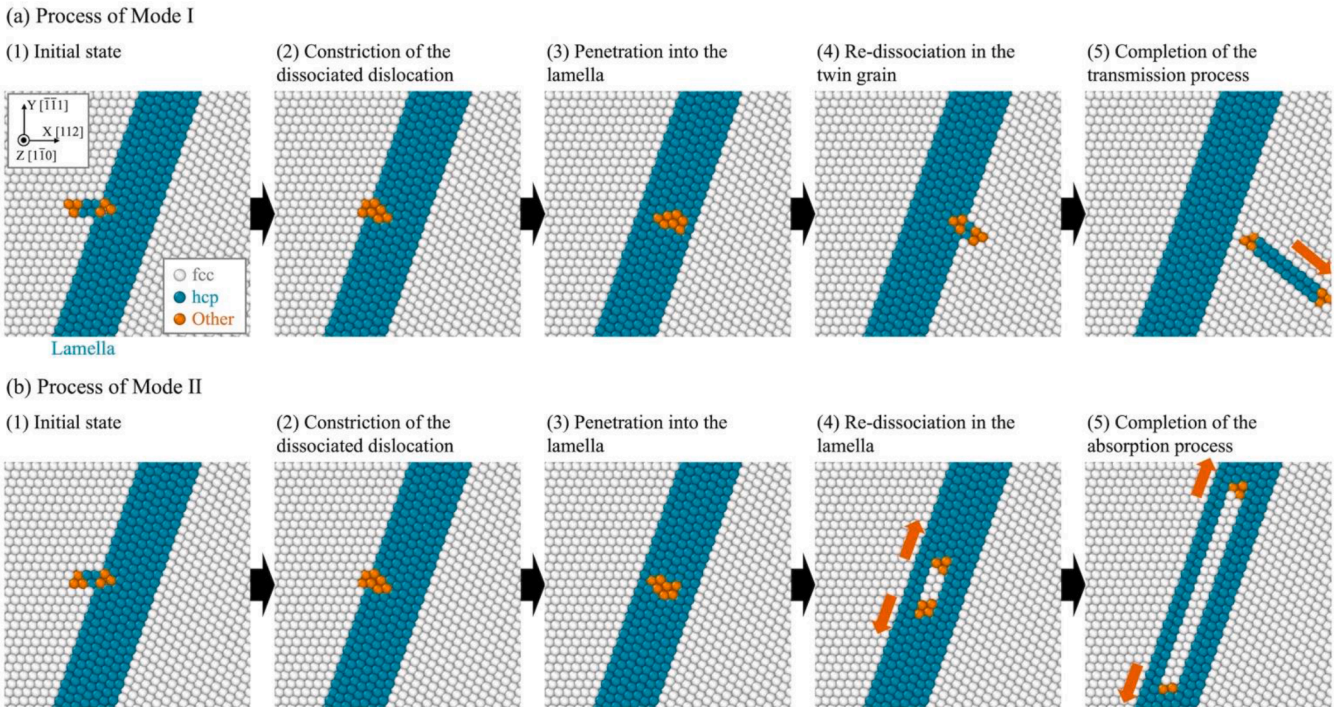

Fig. 2. Two observed interaction processes: (a) Mode I and (b) Mode II. A representative case is shown here for each interaction mode. The processes are visualized by the CNA [30], where white and blue represent atoms with the fcc and hcp structure, respectively, while orange expresses atoms with neither fcc nor hcp structure.

different calculations, which is probably controlled by the local environment of the atomic species within the lamella. For instance, a previous atomistic simulation reported the regional stacking fault energy (γ_{SFE}) significantly fluctuates in Ni-based concentrated alloys due to the local chemical environment [32]. We consider an interaction process as Mode II if the dislocation is absorbed by the lamella, regardless of the point of the re-dissociation. Additionally, we confirm no essential difference in each interaction mode between different systems and repeated calculations. A previous computational study [17] observed Mode I alone for the interaction between a screw dislocation and hcp lamella. This is probably because they employed an interatomic potential for fcc Co with a negative γ_{SFE}. The negative γ_{SFE} results in an unrealistic large separation distance between the partial dislocations (d_{sep}) and high critical stress of the interaction, strongly favoring the occurrence of Mode I (the detailed explanation is given below). In addition, a previous study performed MD simulations for the interaction between a screw dislocation and CTB in pure Ni, NiFe, and NiCoCrFe [10] employing the same potential [28] as this study. While they also observed dislocation transmission and absorption processes, only the dislocation transmission is identified if the temperature is below 100 K, regardless of the system. However, in our simulations (77 K), we observe both Mode I and II, depending on the system. This difference may be because the volume of the hcp region changes through the occurrence of Mode II in our case, as shown in Fig. 2(b), while it does not change in the dislocation–CTB interaction [10]. This would result in a stronger γ_{SFE} dependence of the interaction mode, leading to the occurrence of

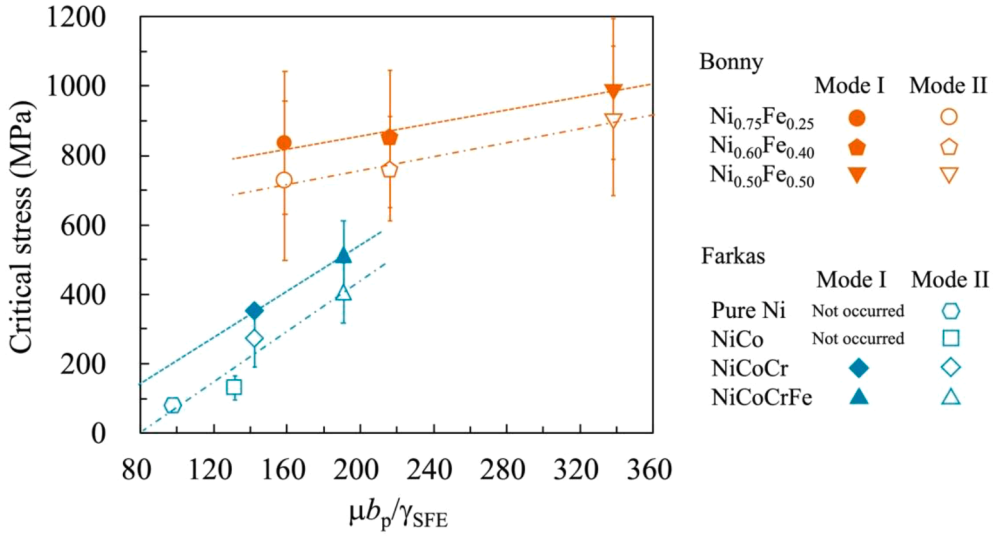

Fig. 3. Critical stress for Mode I and II as a function of $\mu b_p/\gamma_{SFE}$ at the lamella thickness of 7 atomic layers. The dashed and dotted-dashed lines are obtained by the least square method for the stresses of Mode I and II, respectively. The error bars denote the standard deviation of the mean.

different interaction modes in different systems.

Fig. 3 shows the critical stress for Mode I and II as a function of $\mu b_p/\gamma_{SFE}$ at the lamella thickness of 7 atomic layers. Note that μ and b_p represent the shear modulus and Burgers vector of a Shockley partial dislocation, respectively. The critical stress of each mode becomes larger with an increase in $\mu b_p/\gamma_{SFE}$ under the comparison within the same potential. This is because the value of $\mu b_p/\gamma_{SFE}$ corresponds to d_{sep}, according to the elasticity theory [33]:

$$\frac{d_{sep}}{b_p} = \frac{(2-3\nu)}{8\pi(1-\nu)}\frac{\mu b_p}{\gamma_{SFE}} \quad (1)$$

where ν represents the Poisson's ratio. Since the dissociated dislocation needs to be constricted for the onset of the interaction in both Mode I and II, as shown in Fig. 2, the d_{sep} is a controlling factor for the interaction's critical stresses. A similar relationship between the interaction's critical stress and $\mu b_p/\gamma_{SFE}$ was also reported for the interaction between a screw dislocation and CTB [10,26]. In this study, we find Mode I exhibits a higher critical stress than Mode II, where the difference is ~100 MPa, regardless of the value of $\mu b_p/\gamma_{SFE}$ and employed potential.

Fig. 4 shows the ratio of Mode I as a function of the averaged critical stress at each condition in the case of the lamella thickness of 7 atomic layers. Note, the Mode I ratio here expresses the number of Mode I cases divided by the number of all the repeated calculations at each condition. Mode I occurs more frequently as the averaged critical stress becomes higher. In addition, the transition of the dominant mode from Mode II to I is expected to occur at ~500 MPa, as shown in a dashed curve in the figure. As mentioned above, the dislocation transmission and absorption processes were also previously observed for the dislocation–CTB interaction [10,26,34], and it was reported that the type of interaction mode to occur is stress-dependent [26]. Specifically, the dislocation transmission is dominant at over ~400 MPa while the absorption process is favored below it [26]. They confirmed this stress value is not influenced by the employed potential. As shown in Fig. 4, the stress level for the dominant mode transition in [26] is comparable to that observed in this study.

Fig. 5(a) and (b) show the dependence of the critical stress and Mode I ratio on the hcp lamella thickness, respectively. We here show the results of $Ni_{0.75}Fe_{0.25}$ by the Bonny potential and those of NiCoCrFe by the Farkas potential as a representative case for each potential. As shown in Fig. 5(a), the lamella thickness has little influence on the critical stress, regardless of the interaction mode and employed potential. Meanwhile, the Mode I ratio gradually decreases as the lamella becomes thicker for both systems, as shown in Fig. 5(b). We expect the Mode I ratio continues to decrease with a further increase in the thickness. This is because the dislocation would have a higher probability of re-dissociation during the penetration within the lamella by experiencing various local environments of atomic species.

We discuss possible effects of the observed mechanisms and dependences on the strength and ductility of the system in the following. First, as shown in Fig. 3, the critical stress increases as $\mu b_p/\gamma_{SFE}$ becomes larger. This could contribute to a higher strength of the system with decreasing γ_{SFE}. Second, the frequency of Mode I is higher with an increase in the critical stress, as shown in Fig. 4. This suggests the interaction under a high stress condition could lead to a higher ductility of the system. It is because the deformation process can propagate across the lamella through the dislocation transmission in Mode I, while the deformation is accumulated within the original grain through Mode II due to the dislocation absorption. The combination of these two dependences indicates the screw dislocation–hcp lamella interaction could contribute to a simultaneous increase in the strength and ductility at lower γ_{SFE} owing to the higher critical stress, inducing a frequent occurrence of Mode I. Furthermore, an experimental study suggested γ_{SFE} decreases with lowering temperature in NiCoCr [35]. This indicates the interaction could lead to a simultaneous increase in the strength and ductility at lower temperatures in NiCoCr.

We also observe a unique mechanism of Mode II that could further enhance the contribution of the interaction to the ductility, as described in the following. Mode II is considered as a healing process of hcp layers back into fcc phase (Fig. 2 (b-4) and (b-5)), which would lead to rendering the hcp lamella thinner. Note, the healing process by dislocation–hcp lamella interactions was also observed in a previous computational study while it was the case of a mixed dislocation [17]. In addition, experimental studies [17,19] reported the observed fraction of hcp phase under deformation was relatively small in NiCoCr although DFT calculations showed the hcp phase is more stable than the fcc phase

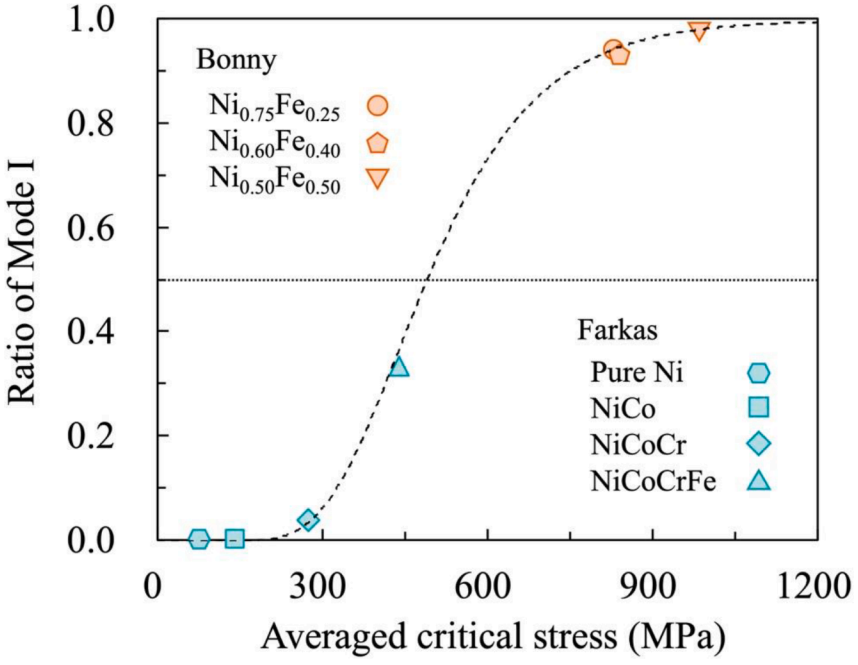

Fig. 4. Ratio of Mode I as a function of the critical stress at the lamella thickness of 7 atomic layers. The critical stress here is taken as the averaged value over all the repeated calculations, regardless of the type of the interaction mode. The dashed curve is a visual guide.

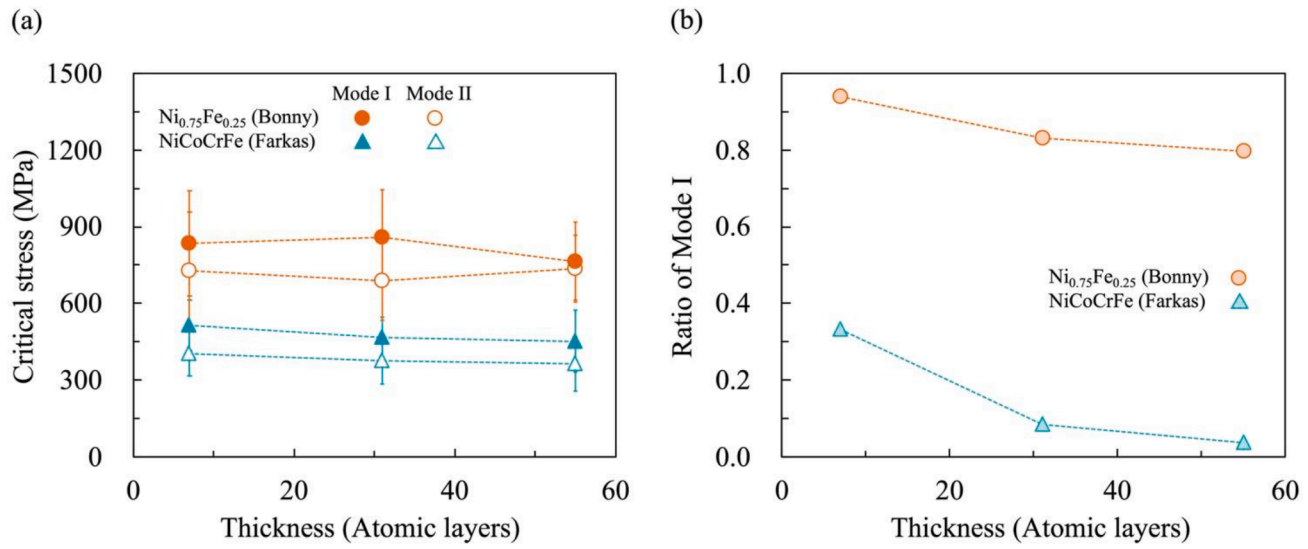

Fig. 5. Lamella thickness influence on (a) the critical stress and (b) Mode I ratio for $Ni_{0.75}Fe_{0.25}$ by the Bonny potential and NiCoCrFe by the Farkas potential. The error bars denote the standard deviation of the mean.

[19]. This might be because dislocation–hcp lamella interactions suppress the growth of hcp lamella through the occurrence of Mode II. Meanwhile, as shown in Fig. 5(b), Mode I occurs more frequently with a decrease in the lamella thickness. This suggests the interaction could lead to an enhanced ductility more at a thinner lamella. Therefore, Mode II is a unique mechanism that could promote the interaction's contribution to the ductility by rendering the lamella thinner.

In summary, we perform MD simulations of the interaction between a screw dislocation and nanotwin–hcp lamella in Ni-based concentrated alloys. Two types of interaction modes are observed, i.e., the dislocation is transmitted across the lamella through Mode I while it is absorbed by the lamella in Mode II. It is found that the critical stress of each mode increases as $\mu b_p/\gamma_{SFE}$ becomes larger regardless of the employed interatomic potentials. In addition, Mode I occurs more frequently with an increase in the critical stress. These dependences could lead to higher strength and ductility at lower temperatures in NiCoCr due to the decreased γ_{SFE}. We observe Mode II heals hcp layers within the lamella back into fcc phase during the process. Furthermore, the frequency of Mode I is higher at a thinner lamella while the lamella thickness does not significantly influence the critical stress of each mode. These indicate dislocation–hcp lamella interactions possess a unique mechanism to render the lamella thinner through Mode II, which could further promote the interaction's contribution to the ductility.

Declaration of Competing Interest

The authors declare no competing financial interests.

Acknowledgments

This work is supported by the National Science Foundation under Grant No. DMR-1654438. This work uses the Extreme Science and Engineering Discovery Environment (XSEDE), which is supported by the National Science Foundation grant number TG-DMR170112.

Supplementary materials

Supplementary material associated with this article can be found, in the online version, at doi:10.1016/j.scriptamat.2022.114810.

References

[1] J.-.W. Yeh, S.-.K. Chen, S.-.J. Lin, J.-.Y. Gan, T.-.S. Chin, T.-.T. Shun, C.-.H. Tsau, S.-.Y. Chang, Adv. Eng. Mater. 6 (2004) 299–303.
[2] E.P. George, D. Raabe, R.O. Ritchie, Nat. Rev. Mater. 4 (2019) 515–534.
[3] E.P. George, W.A. Curtin, C.C. Tasan, Acta Mater 188 (2020) 435–474.
[4] B. Cantor, I.T.H. Chang, P. Knight, A.J.B. Vincent, Mater. Sci. Eng. A 375–377 (2004) 213–218.
[5] B. Gludovatz, A. Hohenwarter, D. Catoor, E.H. Chang, E.P. George, R.O. Ritchie, Science 345 (2014) 1153–1158.
[6] A. Gali, E.P. George, Intermetallics 39 (2013) 74–78.
[7] F. Otto, A. Dlouhy, Ch. Somsen, H. Bei, G. Eggeler, E.P. George, Acta Mater 61 (2013) 5743–5755.
[8] O.N. Senkov, G.B. Wilks, J.M. Scott, D.B. Miracle, Intermetallics 19 (2011) 698–706.
[9] Q. Ding, X. Fu, D. Chen, H. Bei, B. Gludovatz, J. Li, Z. Zhang, E.P. George, Q. Yu, T. Zhu, R.O. Ritchie, Mater. Today 25 (2019) 21–27.
[10] S. Hayakawa, H. Xu, Acta Mater 211 (2021), 116886.
[11] Z. Wu, H. Bei, G.M. Pharr, E.P. George, Acta Mater 81 (2014) 428–441.
[12] Y. Wang, B. Liu, K. Yan, M. Wang, S. Kabra, Y.-.L. Chiu, D. Dye, P.D. Lee, Y. Liu, B. Cai, Acta Mater 154 (2018) 79–89.
[13] Q. Lin, J. Liu, X. An, H. Wang, Y. Zhang, X. Liao, Mater. Res. Lett. 6 (2018) 236–243.
[14] B. Gludovatz, A. Hohenwarter, K.V.S. Thurston, H. Bei, Z. Wu, E.P. George, R. O. Ritchie, Nat. Commun. 7 (2016), 106102.
[15] G. Laplanche, A. Kostka, C. Reinhart, J. Hunfeld, G. Eggeler, E.P. George, Acta Mater 128 (2017) 292–303.
[16] B. Uzera, S. Picak, J. Liu, T. Jozaghi, D. Canadinc, I. Karaman, Y.I. Chumlyakov, I. Kireeva, Mater. Res. Lett. 6 (2018) 442–449.
[17] C. Niu, C.R. LaRosa, J. Miao, M.J. Mills, M. Ghazisaeidi, Nat. Commun. 9 (2018) 1363.
[18] Y. Ma, F. Yuan, M. Yang, P. Jiang, E. Ma, X. Wu, Acta Mater 148 (2018) 407–418.
[19] J. Miao, C.E. Slone, T.M. Smith, C. Niu, H. Bei, M. Ghazisaeidi, G.M. Pharr, M. J. Mills, Acta Mater 132 (2017) 35–48.
[20] C.E. Slone, S. Chakraborty, J. Miao, E.P. George, M.J. Mills, S.R. Niezgoda, Acta Mater 158 (2018) 38–52.
[21] C.E. Slone, J. Miao, E.P. George, M.J. Mills, Acta Mater 165 (2019) 496–507.
[22] H.W. Deng, Z.M. Xie, B.L. Zhao, Y.K. Wang, M.M. Wang, J.F. Yang, T. Zhang, Y. Xiong, X.P. Wang, Q.F. Fang, C.S. Liu, Mater. Sci. Eng. A 744 (2019) 241–246.
[23] C.L. Tracy, S. Park, D.R. Rittman, S.J. Zinkle, H. Bei, M. Lang, R.C. Ewing, W. L. Mao, Nat. Commun. 8 (2017) 15634.
[24] F. Zhang, Y. Wu, H. Lou, Z. Zeng, V.B. Prakapenka, E. Greenberg, Y. Ren, J. Yan, J. S. Okasinski, X. Liu, Y. Liu, Q. Zeng, Z. Lu, Nat. Commun. 8 (2017) 15687.
[25] T. Hatano, Phys. Rev. B 77 (2008), 064108.
[26] M. Chassagne, M. Legros, D. Rodney, Acta Mater 59 (2011) 1456–1463.
[27] G. Bonny, D. Terentyev, R.C. Pasianot, S. Ponce, A. Bakaev, Modelling Simul. Mater. Sci. Eng. 19 (2011), 085008.
[28] D. Farkas, A. Caro, J. Mater. Res. 33 (2018) 3218.
[29] S. Plimpton, J. Comput. Phys. 117 (1995) 1–19.
[30] H. Tsuzuki, P.S. Branicio, J.P. Rino, Comput. Phys. Commun. 177 (2007) 518–523.
[31] A. Stukowski, Model. Simul. Mater. Sci. Eng. 18 (2010), 015012.
[32] L. Xu, L. Casillas-Trujillo, Y. Gao, H. Xu, Comput. Mater. Sci. 197 (2021), 110618.

[33] D. Hull, D.J. Bacon, Introduction to Dislocations, Pergamon, Oxford, 1984 third ed.
[34] Z.-.H. Jin, P. Gumbsch, E. Ma, K. Albe, K. Lu, H. Hahn, H. Gleiter, Scripta Mater. 54 (2006) 1163–1168.
[35] M. Naeem, H. He, F. Zhang, H. Huang, S. Harjo, T. Kawasaki, B. Wang, S. Lan, Z. Wu, F. Wang, Y. Wu, Z. Lu, Z. Zhang, C.T. Liu, X.-.L. Wang, Sci. Adv. 6 (2020) x4002.